RADC-TR-76-158
Final Report
May 1976

STUDY OF ELECTRONIC TRANSPORT AND BREAKDOWN IN THIN INSULATING FILMS

Princeton University

Sponsored by
Defense Advanced Research Projects Agency
ARPA Order No. 2180

ROME AIR DEVELOPMENT CENTER
AIR FORCE SYSTEMS COMMAND
GRIFFISS AIR FORCE BASE, NEW YORK

STUDY OF ELECTRONIC TRANSPORT AND BREAKDOWN IN THIN INSULATING FILMS

Contractor: Princeton University
Contract Number: F19628-72-C-0298
Effective Date of Contract: 1 July 1972
Contract Expiration Date: 30 November 1975
ARPA Order No. 2180
Program Code No. 4D10
Principal Investigator: Prof. Walter C. Johnson
Phone: 609-452-4621
Project Engineer: Dr. John C. Garth
Phone: 617-861-4051

This report has been reviewed by the RADC Information Office (OI) and is releasable to the National Technical Information Service (NTIS). At NTIS it will be releasable to the general public including foreign nations.

This report has been reviewed and is approved for publication.

APPROVED:

John C. Garth

JOHN C. GARTH
Contract Monitor

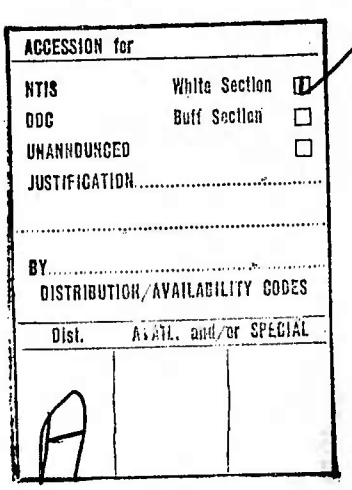

Do not return this copy. Retain or destroy.

Unclassified

SECURITY CLASSIFICATION OF THIS PAGE (When Data Entered)

REPORT DOCUMENTATION PAGE

READ INSTRUCTIONS BEFORE COMPLETING FORM

1. REPORT NUMBER: RADC-TR-76-158	2. GOVT ACCESSION NO.
3. RECIPIENT'S CATALOG NUMBER	
4. TITLE (and Subtitle): STUDY OF ELECTRONIC TRANSPORT AND BREAKDOWN IN THIN INSULATING FILMS.	5. TYPE OF REPORT & PERIOD COVERED: Final Rept. 1 July 1972 - 30 Nov 1975
	6. PERFORMING ORG. REPORT NUMBER
7. AUTHOR(S): Walter C. Johnson	8. CONTRACT OR GRANT NUMBER(s): F19628-72-C-0298; ARPA Order-2180
9. PERFORMING ORGANIZATION NAME AND ADDRESS: Princeton University, Department of Electrical Engineering, Princeton, New Jersey 08540	10. PROGRAM ELEMENT, PROJECT, TASK AREA & WORK UNIT NUMBERS: 61101D, 5621, 562109, 56210901
11. CONTROLLING OFFICE NAME AND ADDRESS: Defense Advanced Research Projects Agency, 1400 Wilson Blvd., Arlington, VA 22209	12. REPORT DATE: May 1976; 13. NUMBER OF PAGES: 45 (48 p.)
14. MONITORING AGENCY NAME & ADDRESS (if different from Controlling Office): Deputy for Electronic Technology (RADC/ETSR), Hanscom AFB MA 01731, Attn: Dr. John C. Garth	15. SECURITY CLASS. (of this report): Unclassified
	15a. DECLASSIFICATION/DOWNGRADING SCHEDULE

16. DISTRIBUTION STATEMENT (of this Report)

A - Approved for public release; distribution unlimited.

17. DISTRIBUTION STATEMENT (of the abstract entered in Block 20, if different from Report)

16 AF-5621 17 562109

18. SUPPLEMENTARY NOTES

This research was supported by the Defense Advanced Research Projects Agency. ARPA Order No. 2180. Work is continuing under ARPA Order No. 2182, monitored by the U.S. Army Night Vision Laboratory.

19. KEY WORDS (Continue on reverse side if necessary and identify by block number)

Dielectric Breakdown
Insulating Films
Corona-Induced Breakdown
Self-Quenched Breakdown
Silicon Dioxide

20. ABSTRACT (Continue on reverse side if necessary and identify by block number)

Results are reported on a set of studies of high-field electronic injection, transport, trapping, and dielectric breakdown in thin (500-5000 Å) films of silicon dioxide thermally grown on silicon substrates. The studies include corona-induced high field injection and transport, self-quenched breakdown, effects of electron irradiation, study of charge-carrier trapping, study of lateral nonuniformities by electrical measurement techniques and by use of a scanning electron microscope, and the theoretical modeling of hot-electron transport and of localized breakdown.

DD FORM 1 JAN 73 1473 EDITION OF 1 NOV 65 IS OBSOLETE S/N 0102-014-6601

Unclassified

SECURITY CLASSIFICATION OF THIS PAGE (When Data Entered)

409 421

TABLE OF CONTENTS

ACKNOWLEDGEMENTS

Acknowledgement is due to Professor Murray A. Lampert for the many contributions that he made to the work reported here. Professor Lampert was Principal Investigator on this project from July 1, 1972 until December 31, 1973, and has been a consultant on this work since that time. Acknowledgement is also made to Dr. W. R. Bottoms, who guided the scanning-electron-microscope studies of interfaces.

Many of our samples were fabricated at the RCA Laboratories, and we thank the many staff members of that organization who made this possible.

1. INTRODUCTION

This report summarizes the results obtained in a research program directed toward a basic understanding of electronic transport, charge trapping, and dielectric breakdown in thin (500-3000 A) silicon dioxide films thermally grown on silicon substrates. The research techniques that we have developed and utilized are applicable to other insulating films, but up to this time we have concentrated on the properties of thermally grown SiO_2 films because of the importance of the Si/SiO_2 system in modern solid-state circuits. The purpose of the program was to provide a correct and quantitatively accurate understanding of the physical processes taking place under high-field conditions in these films, with the ultimate objective of providing a rational basis for the choice of processing methods and treatment of the insulating films for increased yield in manufacturing and greater reliability in use.

The work of this program has resulted in a number of doctoral dissertations, reports, and publications in the periodical literature (see References 1-19 at the end of this report).

The program consisted of a number of coordinated investigations which included studies of charge injection, transport, and trapping in which the injection of charge carriers into the insulator was induced by corona charging of the surface of the insulator, the study of the instability at the onset of breakdown and of catastropic breakdown itself by the self-quenching technique, the probing of trapping centers in the insulating film by charge-discharge techniques using equipment which we developed especially for this purpose, studies of charge transport and trapping using an electron beam for carrier injection, studies of lateral nonuniformities in MIS structures by electrical measurement techniques and by use of a scanning electron microscope, and theoretical modeling of hot-electron transport and of localized breakdown. Separate sections of this report are devoted to each of these studies.

2. HIGH FIELD EFFECTS STUDIED BY CORONA CHARGING

(Z. A. Weinberg and H. S. Lee collaborating)

2.1. Introduction

The study of charge-carrier transport in insulating films requires means of carrier injection and the application of an electric field to the insulator. When a conventional metal-insulator-semiconductor (MIS) structure is used, a localized breakdown will provide a path for discharge of the electrostatic energy of the entire capacitor-like structure and the sample may be permanently damaged. As has been shown by Williams and Woods,[20] this problem can be circumvented if the surface of the insulator is left unmetallized and is electrically contacted with suitable ions of low kinetic energy. Under conditions of small lateral conductivity on the exposed insulator surface, both the total current and the local current density are strongly limited. Runaway breakdown is thus avoided and, in addition, measurements made under these conditions are insensitive to the presence of small weak spots and yield results which, to a good approximation, are representative of the principal, uniform portions of the film.

We have developed techniques in which ions extracted from a corona discharge are used to induce charge injection and transport in thin insulating films for the purpose of studying high-field transport without destructive breakdown,[1,2] and we have applied these methods to a study of SiO_2 films thermally grown on silicon substrates.[8,18] The techniques include a comparison method for measurement of the voltage across the insulator during steady-state corona charging[10] and a shallow p-n junction method for determination of the sign of the principal charge carrier in the insulator.[5] The vibrating Kelvin probe technique was used to measure the decay of insulator surface potential following the cessation of surface charging. This technique, by virtue of its sensitivity and accuracy, provided unusually reliable data for studying the tunneling of electrons from the silicon substrate into the SiO_2.

The principal advantages of the corona method are the availability of either positive or negative ions and the small, essentially thermal, kinetic energy of the ions owing to their short mean free path (about 10^{-5} cm) in the gas at atmospheric pressure. The latter point is of considerable

significance because ions that strike the SiO_2 surface at kinetic energies of tens of eV or higher can damage the surface and can even produce damage at the Si-SiO_2 interface.

Of particular interest are the basic injection processes that may occur when ions of negligible kinetic energy are neutralized at the surface of an insulator. A qualitative band diagram for the ion-SiO_2-Si system is shown in Fig. 1. The energy of the ionic charge relative to the bands in the SiO_2 is indicated by the vertical positions of the + and - signs for positive and negative ions, respectively. The diagram shows two possibilities: For ions of type A, the ionic energy state faces the insulator conduction or valence band; hence the excess charge can be injected directly into the band, after which the carrier may be either trapped or transported through the insulator. For ions of type B, the ionic energy state lies opposite the forbidden gap of the insulator and injection through a barrier is necessary. This process requires the buildup of a large electric field across the insulator so that, in the steady state, the barrier-limited injection current will equal the ionic current arriving at the surface. If the field across the SiO_2 film is sufficiently high, carriers may be injected by tunneling from the silicon conduction or valence bands. Thus, either holes or electrons may be transported through the insulator for either polarity of the ions.

2.2. Experimental Methods

The general arrangement for the experiments was dictated by the requirement of having a controlled and reproducible atmosphere. This was achieved by housing the sample and the experimental probes in an environmental chamber in which the relative humidity was kept below 2%. The corona discharge was produced by applying a dc voltage of up to 5 kV to a gold-plated tungsten needle which was positioned vertically, point downward, at a distance of about 2.5 cm above the sample. The polarity of the voltage determines the sign of the ions that are drifted to the surface of the sample. The sample current was controlled by varying either the voltage applied to the corona-forming electrode or the potential of a coarse grid of wires interposed between the corona discharge and the sample. The arrangement was capable of supplying sample currents of up to a few $\mu A/cm^2$.

The potential difference across the insulating film was measured during steady-state charging by a comparison technique,[10] and the surface potential of the sample after cessation of charging was monitored by use of a vibrating Kelvin probe. The principle of the comparison technique is shown in Fig. 2. The method is based on the dynamics of ions when drifting under collision-dominated conditions: their trajectories follow, to a close approximation, the electrostatic field lines. A grounded metal reference plate and the sample are arranged symmetrically beneath the corona discharge, and the top surface of the insulating film is brought to ground potential by adjusting the dc source, V_B, until the two currents, I_i and I_m, are equal. The voltage V_B is then equal to the potential difference across the insulator. Further details of the technique are provided in Ref. 10. The best resolution obtainable by use of this method in our experiments was about $\pm$ 1 V.

The vibrating Kelvin probe, which was gold plated, had a diameter of 5 mm and was spaced about 1 mm from the surface of the insulator. It was vibrated at 400 Hz, and the signal was detected by a lock-in detector. The arrangement had a resolution of $\pm$ 0.05 V.

A measure of the charge retained in the oxide after corona charging was obtained from the high-frequency (1-MHz) capacitance-voltage (C-V) characteristic, using a mercury probe for temporary metallization of the insulator surface.

2.3. Identification of Carrier Sign

A clear determination of the sign of the dominant charge carrier transported across the insulating film was of vital importance to this study. A technique that proved to be particularly illuminating was the use of the charge-separating properties of a shallow p-n junction detector incorporated into the semiconductor substrate.[5] The principle of operation is illustrated in Fig. 3. To avoid inversion of the thin layer near the interface with the insulator, a p-type diffusion into an n-type substrate is used for negative corona charging and the reverse of this is used for positive corona charging. Carriers injected from the insulator into the semiconductor are of the same polarity as the corona ions and, as shown in Fig. 3, they enter the thin semiconducting layer as minority carriers. They diffuse through the shallow layer and are collected by the substrate

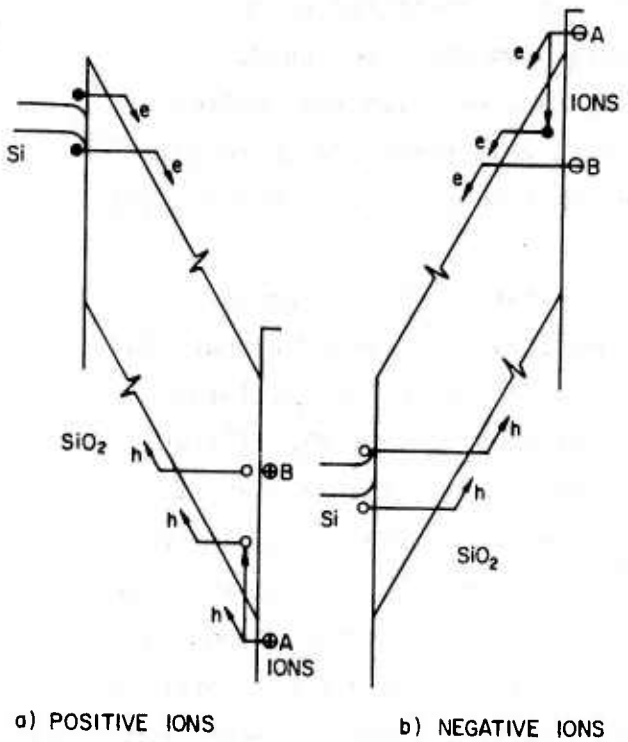

Fig. 1. Schematic illustration of various processes of injection resulting from ion neutralization at the SiO_2 surface. For ions labeled A the energy state faces a band of the SiO_2. For ions labeled B the energy state faces the band gap.

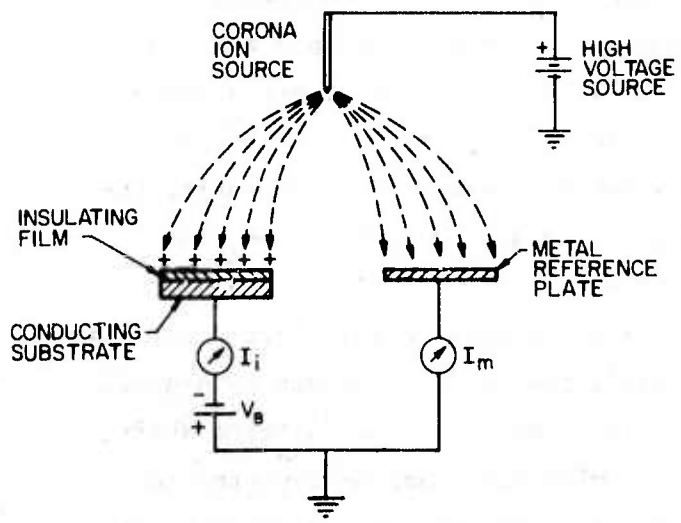

Fig. 2. Basic principle of operation of the comparison technique for measuring the potential difference across the insulating film during steady-state corona charging. The applied voltage V_B is adjusted until $I_i = I_m$, at which point the voltage V_i across the insulator is equal to V_B.

in the same manner as a bipolar transistor. These carriers will give rise to a current in the external circuit that is connected to the substrate [I_n in Fig. 3(a), I_p in Fig. 3(b)]. On the other hand, majority carriers of opposite sign that are injected from the shallow semiconducting region into the insulator will give rise to a current in the external circuit that is connected to the thin layer [I_p in Fig. 3(a), I_n in Fig. 3(b)].

The shallow junction detector has also proved to be a powerful instrument for monitoring charge-carrier multiplication effects that can take place in the semiconductor near its interface with the insulator. When electrons are injected from thermally grown SiO_2 into the silicon substrate [Fig. 3(a)], they enter the silicon with at least 3.1 eV of excess kinetic energy, corresponding to the barrier height between the silicon and SiO_2 conduction band edges.[20] This excess energy is sufficient to give rise to electron-hole pair production in the silicon. Almost all of the pairs so generated will be separated by the diode and will produce corresponding currents in both sides of the junction. Thus, observation of the magnitude and direction of both currents gives information regarding the physical processes underlying the mechanisms of charge transport.

We performed p-n diode detector experiments using SiO_2 films which were grown in dry oxygen at a temperature of 1000°C to a thickness of approximately 1000 Å. The substrates were 5-Ω cm silicon into which, prior to oxidation, had been diffused an 0.5-μm layer of opposite conductivity type having a surface impurity concentration of 10^{17} - 10^{18} cm^{-3}. The experimental details have been described elsewhere.[5] Our results indicated that electrons were the principal charge carriers in SiO_2 for both polarities of the corona, as follows:

For positive corona, current was observed only in the circuit connected to the n side of the junction [Fig. 3(b)], indicating electron transport. C-V curves taken after positive corona charging showed no flatband shift, consistent with the negligible amount of electron trapping expected in thermally grown SiO_2[21] and inconsistent with the transport of holes, for the latter would be accompanied by hole trapping and a buildup of positive charge in the oxide.

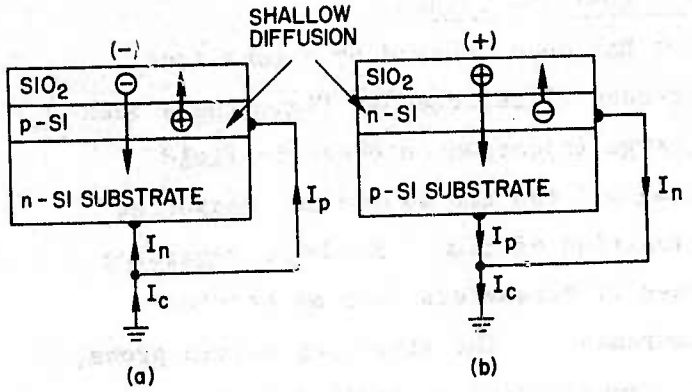

Fig. 3. Schematic illustration of the shallow p-n junction technique for determination of the sign of charge carrier: (a) for negative insulator surface potential, (b) for positive insulator surface potential. I_c is the corona current reaching the diode.

For negative corona, currents were observed in both circuits, with $I_n \approx 2I_c$ and $I_p \approx -I_c$ [Fig. 3(a)].[5] We interpret this as indicating that each electron entering the silicon from the SiO_2 generates, on the average, approximately one electron-hole pair by impact ionization, as was described above.

2.4. Steady-State Current-Voltage Characteristics

The comparison technique described in Sec. 2.2 permits simultaneous measurement of current and potential difference across the insulating film. Typical results obtained on silicon dioxide films thermally grown on silicon substrates are shown in Fig. 4 for corona charging in an atmosphere of dry air. The SiO_2 films were HCl-steam grown at 900°C on (100) silicon of 1-2 ohm-cm resistivity. Both p and n substrates were used. The range of thicknesses of the SiO_2 films was 580-2580 Å as measured by ellipsometry. Both polarities of corona charging were used. Within the limits of error shown by the error bars in Fig. 4, substantially identical results were obtained for both n and p substrates. In the upper part of the curves, corresponding to about one decade of rapidly increasing current, the variation in electric field was sufficiently small to permit definition of an approximate value of nondestructive breakdown field. The thickness dependence of this is shown in Fig. 5.

Within the limits of error, the values of these fields are in agreement with Kelvin-prove measurements made immediately upon cessation of the corona charging and also with the results reported by Williams and Woods.[20]

2.5. Surface Potential Decay Studies. Positive Corona

After the surface of an insulator has been charged by corona ions and one or more of the injection processes illustrated in Fig. 1 have been established, the dependence of the charge injection on electric field intensity can be determined by shutting off the ion source and measuring the decay of surface potential as a function of time. Evidence regarding the injection mechanisms and the values of parameters such as barrier height can be deduced from these measurements. The vibrating Kelvin probe, by virtue of its high resolution and insensitivity to small defects, provides an unusually accurate means of measuring insulator surface potential in such studies. Representative results obtained with position-ion surface charging are given in this section, and the results of negative-ion charging are discussed in the following section.

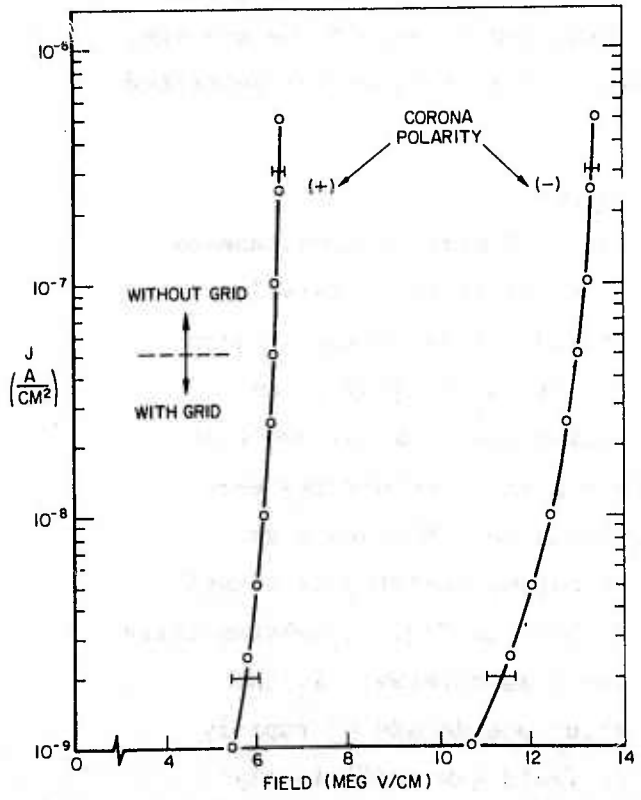

Fig. 4. Steady-state current-field characteristics for a 1000-Å film of SiO_2, obtained by the comparison technique (Fig. 2). The lower levels of current are controlled by adjusting the potential of a grid interposed between the corona source and the sample, and the higher levels are controlled by varying the voltage applied to the corona needle.

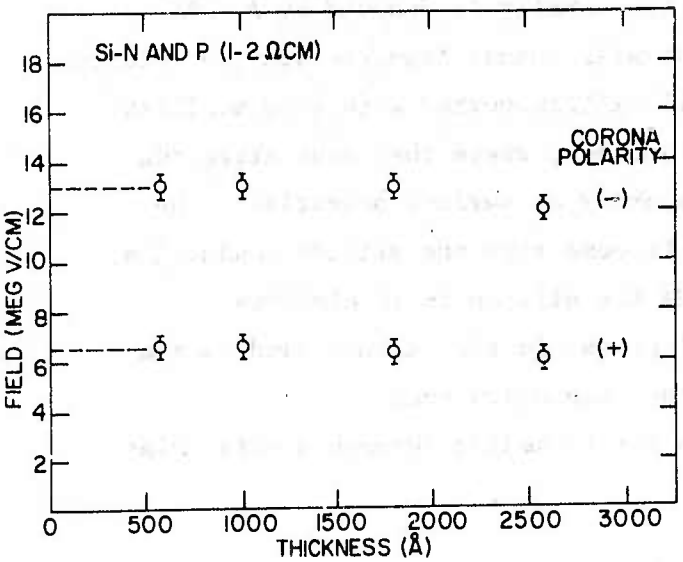

Fig. 5. Thickness dependence of the nondestructive breakdown fields.

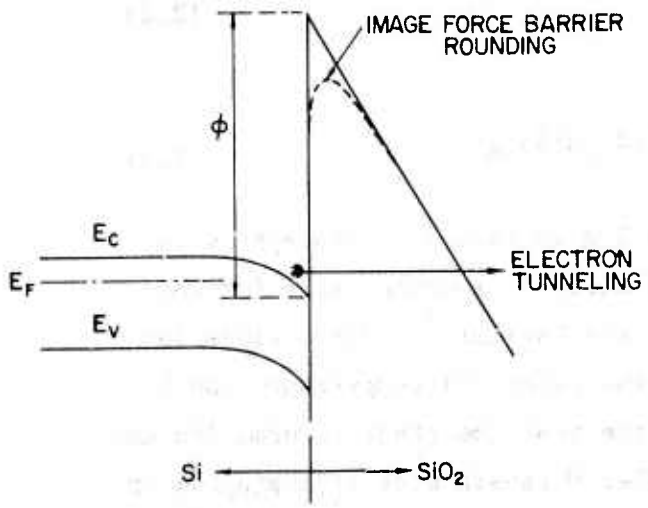

Fig. 6. Schematic band diagram for electron tunneling from the silicon conduction band into the silicon-dioxide conduction band.

Figure 6 shows a schematic diagram of the energy bands in the vicinity of the Si-SiO_2 interface when the surface of the insulator is positively charged. The height of the barrier is denoted by ϕ. At sufficiently large fields, electrons will tunnel from the silicon into the conduction band of the SiO_2 and will be transported with good mobility ($\mu_n \sim 20$ cm^2/V-sec)[22] to the front surface, where they neutralize the positive surface charge and cause a decay of surface potential. The tunneling electrons can be assumed to come from the silicon conduction band only, since at tunneling fields the silicon is in electron degeneracy at the interface, and electrons in the valence band face a much larger barrier than those in the conduction band.

The Fowler-Nordheim expression for tunneling through a triangular barrier is[23]

$$J = CF^2 \exp(-\beta/F) \tag{2.1}$$

where J is the current density and F is the electric field intensity. To a first approximation,

$$C = \frac{q^2}{8\pi h\phi} \tag{2.2}$$

and

$$\beta = 4(2qm^*)^{1/2} \phi^{3/2}/3\hbar \tag{2.3}$$

where q is the electronic charge, $h = 2\pi\hbar$ is Planck's constant, ϕ is the barrier height in eV, and m^* is a suitably average value for the effective mass of the electron within the barrier.[24] Corrections for image-force barrier rounding and for the effect of temperature can be found in the literature.[23] However, the most important information can be obtained from the slope of the Fowler-Nordheim plot of $\log(J/F^2)$ vs $1/F$:

$$\frac{d(\ln J/F^2)}{d(1/F)} = -\frac{4}{3\hbar}(2qm^*)^{1/2} \phi^{3/2} s(y) \tag{2.4}$$

where s(y) is a slope-correction function[23] and y is the fractional amount of the image-force barrier lowering:

$$y = (qF/4\pi\varepsilon)^{1/2}/\phi \qquad (2.5)$$

In our work the slope-correction factor, s(y) was of the order of 0.99 and could be neglected. Thus, to a good approximation the Fowler-Nordheim slope is equal to β as given by Eq. (2.3).

The decay of electric field in the oxide, caused by the decay in surface charge, is related to the conduction current, J, through the oxide by the expression

$$J = -\varepsilon_{ox} \frac{dF(t)}{dt} \quad , \qquad (2.6)$$

where ε_{ox} is the dielectric permitivity of the oxide. The elimination of J between Eqs. (2.1) and (2.6) yields the following differential equation:

$$-[\beta/F^2(t)]\exp[\beta/F(t)]dF = A\ dt, \qquad (2.7)$$

where

$$A = C\beta/\varepsilon_{ox} \ . \qquad (2.8)$$

Integration of Eq. (2.7) provides the result

$$\ln A(t + t_o) = \beta[1/F(t)], \qquad (2.9)$$

where t_o is a constant of integration defined by the initial value of field, F(0).

We see from Eq. (2.9) that for $t >> t_o$, a plot of log t vs 1/F should result in a straight line with the slope β. If this straight line is extrapolated down to 1/F(0), the value of t_o can be read off the time axis. If the data are then replotted with this value of t_o added to each experimental value of time, the result will be a curve of $\log(t + t_o)$ vs 1/F which should be a straight line of slope β throughout its entire length.

Note that this slope is the same as that obtained in the conventional Fowler-Nordheim plot of log J/F^2 vs $1/F$.

Figures 7 and 8 show typical results of surface-potential decay measurements made after surface charging by positive corona. The SiO_2 films were grown in dry oxygen on n-type (100) silicon substrates with resistivities in the range of 1-2 ohm-cm. The results are shown in Fig. 7 for charging done with ions formed by the corona in a nitrogen atmosphere, and Fig. 8 compares these results with those obtained by charging in helium and dry-air atmospheres. Two oxide thicknesses were used: 1000 Å for charging in nitrogen and in helium, and 559 Å for charging in dry air. Similar results were obtained with oxides of other thicknesses and with samples having p-type substrates. Excellent reproducibility was found among many samples cut from the same wafer, showing the insensitivity of the method to small defects.

The data of Figs. 7 and 8 fit Eq. (2.9) with the constant of integration, t_o, of the order of 1 sec, which is a negligible correction. The results thus confirm the assumption of tunneling from essentially a single energy level. Using Eq. (2.3) and a barrier height of 3.1 eV from the silicon conduction band to the oxide conduction band,[20] the effective mass is calculated to be $m^* = 0.43\ m_o$, where m_o is the free electron mass. This is in reasonable agreement with the value of $0.42\ m_o$ obtained by Lenzingler and Snow[25] using a conventional MOS structure. The independence of the results on the gas ambient, shown in Fig. 8, provides further confirmation that the charge-injection process which discharges the surface takes place entirely at the silicon-oxide interface. We conclude that with positive corona charging of the front surface, the charge injection mechanism into the oxide is the tunneling of electrons from the conduction band of the silicon into the conduction band of the SiO_2.

2.6. Studies With Negative Corona

A. Positive Charge Buildup in the Oxide

When the surface of a silicon dioxide sample is charged by negative corona to a sufficiently high potential, a buildup of positive stored charge is observed in the oxide. By limiting the surface potential

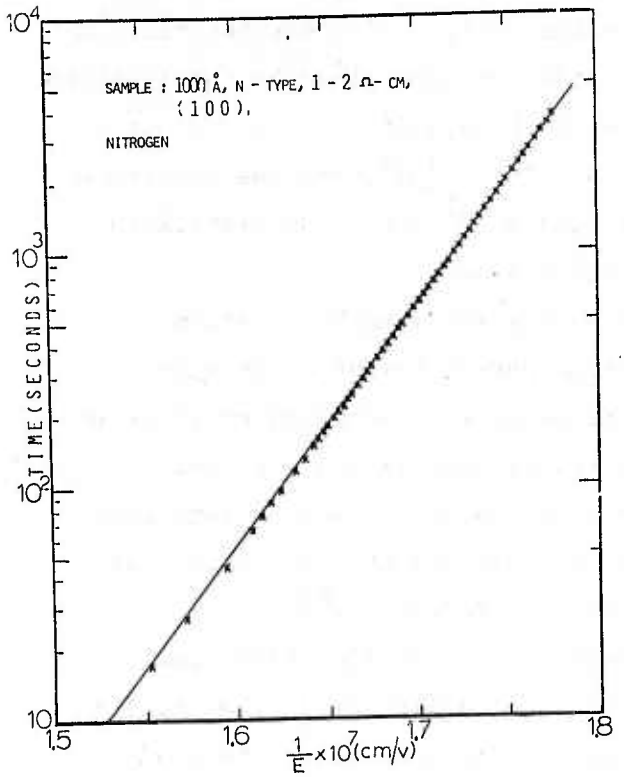

Fig. 7. Decay of electric field in the oxide of a sample with n-type substrate after positive corona is shut off.

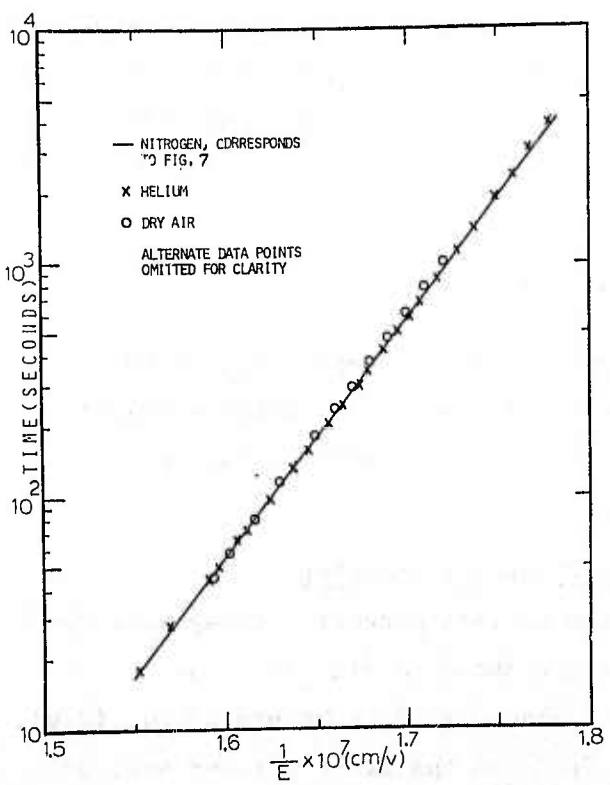

Fig. 8. Discharge of sample after positive corona charging in three gaseous ambients. The oxide thickness was 1000 Å for the dry air. The substrates were n-type (100) Si, 1-2 Ω-cm.

with a grid, a threshold field of $(1.1 \pm 0.1) \times 10^7$ V/cm was found for the appearance of the stored positive charge. Figure 9 shows the buildup of positive charge in a 1000-Å sample of SiO_2 as determined by the flatband shift of C-V curves taken at intervals with the aid of a mercury probe. The corona current was held constant at 5×10^{-7} A/cm^2, and the magnitude of the initial uniform field was $(1.3 \pm 0.1) \times 10^7$ V/cm. No significant differences were found between n and p substrates.

The positive charge can be electronically annealed by injecting electrons into the oxide either by internal photoemission or by subsequent application of positive corona to cause the tunneling of electrons from the substrate (Sec. 2.5). The electronic annealability of the charge indicates that it is caused by trapped holes and not by ions such as sodium. Recent etch-off experiments by Woods and Williams show that the trapped holes are located near the Si-SiO_2 interface.[26]

In attempting to deduce the mechanisms of charge injection from I-V relationships, it is necessary to know the magnitudes of the electric fields at both of the insulator interfaces. With the surface charged negatively and with positive charge storage near the Si-SiO_2 interface, the electric field throughout the main portion of the insulator can be obtained with good accuracy by dividing the voltage across the insulator by the insulator thickness. In the one-dimensional approximation, the electric field at the Si-SiO_2 interface can be obtained from the well known relation

$$E_i = (V_s + V_{FB})/x_{ox} \tag{2.10}$$

where V_s is the magnitude of the voltage across the sample, V_{FB} is the flatband voltage of the structure (negative for positive charge storage), and x_{ox} is the thickness of the oxide. The flatband voltage can be obtained with the aid of a mercury probe.

B. Surface Potential Decay Studies (Negative Charging)

Typical results obtained from surface potential decay measurements after charging with negative ions are shown in Fig. 10. The values of current were obtained from the discharge data by use of Eq. (2.6). The graphs are plotted in terms of the field at the Si-SiO_2 interface, as

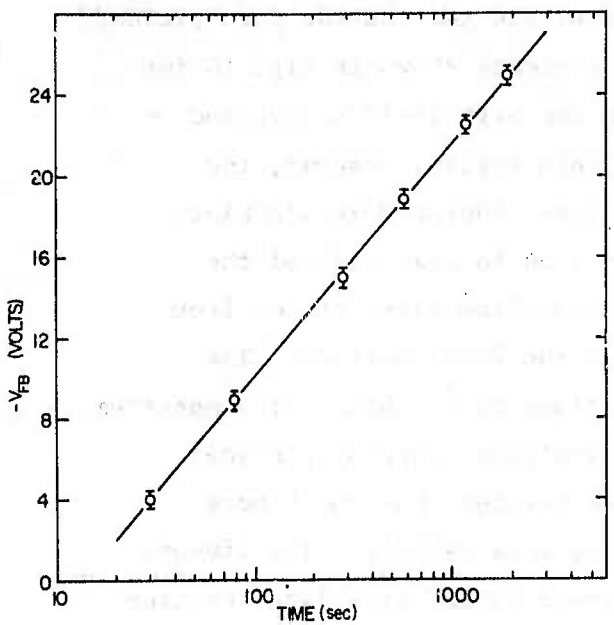

Fig. 9. Positive charge buildup in the SiO_2 during exposure to negative corona, as shown by the shift in flatband voltage of C-V curves taken with a mercury probe. The thickness of the SiO_2 was 1000 Å and the corona current was fixed at 5×10^{-7} A/cm^2.

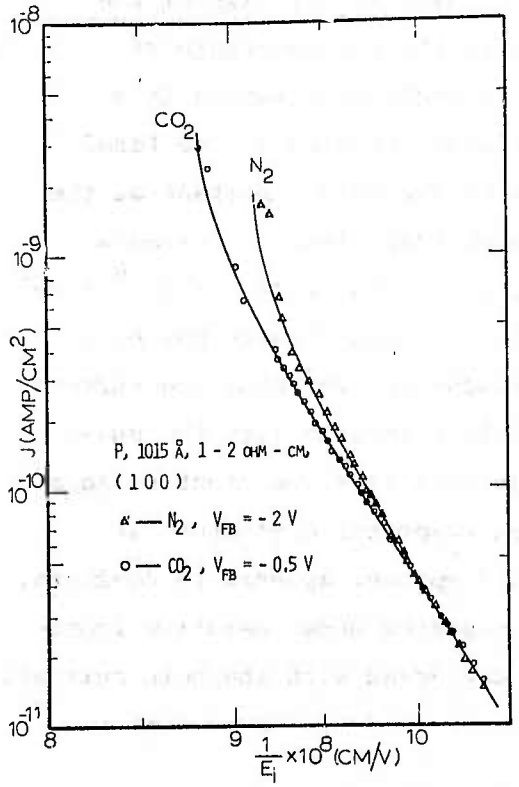

Fig. 10. Showing the effect of the gaseous ambient in which the negative corona is produced.

obtained by Eq. (2.10). Unlike the results obtained after positive-ion charging, where the current is independent of the gas and the data yielded a straight-line Fowler-Nordheim plot, the currents shown in Fig. 10 for negative ion charging are gas-dependent in the high field region and do not plot as a straight line. In the low-field region, however, the currents are gas-independent and yield a linear Fowler-Nordheim plot. The gas dependence obtained at high fields (the initial part of the discharge) would be expected for electron tunneling from ions or from surface states associated with such ions at the front surface. The nonlinear plot of log J vs 1/E can be explained on the basis of a spectrum of energies for trapped electrons, since electrons trapped at higher energies on the surface will face a smaller barrier than those more deeply trapped and will therefore be emitted more rapidly. The linear, gas-independent relationship obtained at lower fields (the later portion of the discharge), when these data are plotted in terms of the field at the Si-SiO_2 interface, indicates that hole injection may be taking place at this interface. In order to confirm this interpretation we used the shallow p-n junction technique (Sec. 2.3) to identify the sign of the carriers. The experiments were carried out in the current range of approximately 10^{-8} - 10^{-7} A/cm^2. The results indicated that in this range the hole currents comprised an appreciable fraction of the total oxide current but that the electron current became more important at the higher current densities. Weinberg[5] has shown that electron currents dominate at still higher current densities, in the range 10^{-7} - 10^{-6} A/cm^2.

We conclude that when the surface of the silicon dioxide has been charged with negative ions and allowed to discharge, the observed current consists of two components, one caused by hole injection from the substrate and the other caused by electron injection from the front surface. At the larger values of current the electron component dominates; at smaller current densities the hole-produced component appears to dominate. The positive charging of the oxide that is observed under negative front-surface charging conditions is undoubtedly connected with the hole currents that we observe.

2.7. Generation of Electron Traps Under High-Field Conditions

It is generally tacitly assumed that the charge-trapping characteristics of an insulating film are determined at the time of formation of the film and remain substantially constant throughout the life of the insulator. Our corona studies show clearly that this is not correct but that, instead, substantial concentrations of charge-trapping centers can be generated under high-field conditions. This provides an explanation for unexpected long-term difficulties that have been observed in MOS devices and opens an area that deserves further careful study.

Thermally grown silicon dioxide normally has only small concentrations of electron traps,[21] typically of the order of 3×10^{14} cm^{-3}. The results of a series of experiments showing the high-field generation of electron traps are shown in Fig. 11. The sample had a p-type (100) substrate, 10 ohm-cm, with a 1950 Å layer of dry-grown silicon dioxide. The first C-V curve of Fig. 11 is for the sample in its original condition. Exposure to positive corona (in dry air) produced an injection of electrons from the substrate into the oxide (Sec. 2.5) and resulted in Curve 2, which shows very little change from Curve 1. The sample was then exposed to

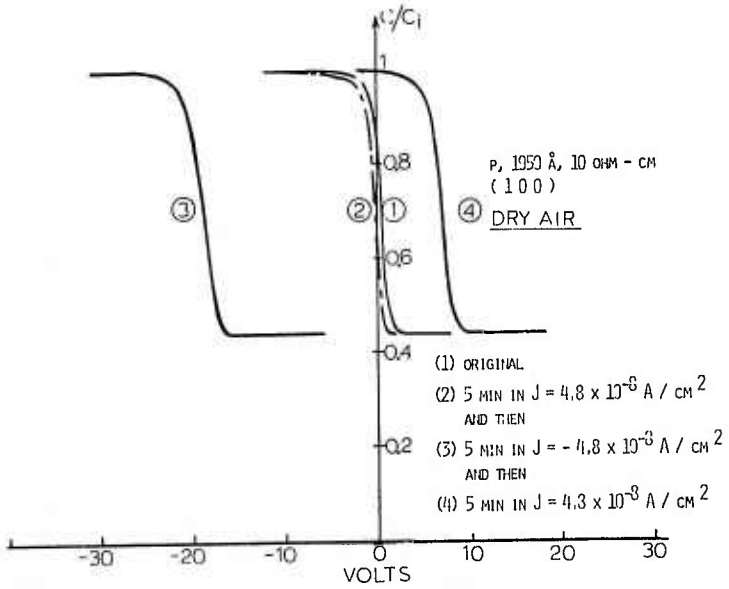

Fig. 11. C-V curves showing typical results obtained by negative corona charging followed by positive corona charging. Negative charge trapping is shown by the positive flat-band shift.

negative corona, and the negative shift of Curve 3 shows a buildup of positive charge (Sec. 2.6A). The remarkable result of this study is seen when the sample is exposed again to positive corona. As is shown by Curve 4, not only is the positive charge neutralized by the resulting injection of electrons, but now there is a substantial trapping of electrons as indicated by the shift of the C-V curve to the right of its original position. The substantial electron trapping revealed in Curve 4, as compared with the small amount of charge trapping shown by Curve 2, is clearly the result of the intermediate step in which the sample was charged to a high electric field by the negative corona. Annealing experiments showed that if the surface was discharged and the sample annealed at 150°C for 30 minutes in vacuum, the traps were discharged but could be charged again by injecting electrons into the oxide. Further annealing experiments showed that the traps themselves disappeared if the anneal was performed at an oxide field of approximately 5×10^6 V/cm.

The physical nature of the electron traps is not known, nor are the precise conditions for their formation. Indeed, we have not investigated their rates of formation, and we do not know whether the trap concentrations that we have observed are saturated values or only intermediate ones. In view of the practical importance of the phenomenon, further study is clearly indicated.

3. HIGH FIELD EFFECTS STUDIED BY THE SELF-QUENCHING TECHNIQUE

(D. Y. Yang collaborating)

3.1. Introduction

The self-quenching technique for studying dielectric breakdown in thin insulating films employs a thin metallization, typically 200-1000 Å in thickness, so that when a localized breakdown occurs in the film, the Joule heat evolved in the immediate vicinity of the fault results in the removal of the metal about this point; thus the damage is self limiting. There are several advantages to this procedure: (1) The remainder of the sample is preserved for further experimentation. (2) The location of the breakdown can be correlated with other information, for example with the location of faults in the substrate, insulator, or metallization. (3) The physical appearance of the breakdown region can provide information about the mechanisms and progress of the breakdown. (4) If the sample originally has weak spots, these can be "blown out" at the start of the experiment and the intrinsic properties of the insulator can then be observed.

The foregoing technique has been used in the past by N. Klein and his co-workers.[27] Here we report on the topography of self-quenched breakdown (SQBD) regions in Al-SiO_2-(100) Si structures, with particular emphasis on an anisotropy that reflects the underlying crystal structure, and on the observation of a slow, high-field instability that is enhanced at lowered temperatures.

3.2. Topography of Self-Quenched Breakdown Regions

The topographic features of SQBD regions produced in Al-SiO_2-(100) Si structures show striking differences among the four possible combinations of substrate type (n or p) and field-plate polarity. The differences are visible in breakdowns produced at room temperature but are more easily seen when the breakdown is induced at reduced temperatures.

The breakdown regions shown in Figs. 12 and 13 were produced in vacuum on 2500-Å SiO_2 which had been HCl-steam-grown on (100) silicon of 1-2 Ω-cm resistivity. The field plates were of aluminum, approximately 1000 Å in thickness. Bias-temperature stress measurements indicated negligible contamination with sodium. Figure 12 shows typical breakdown regions produced at a temperature of 100°K in oxide grown on n-type silicon. The application of positive field-plate voltage (∿ 185 volts) resulted in the

round, smooth breakdown regions, and the application of negative field-plate voltage (∿ 180 volts) produced the irregular breakdown regions. These regions, which print dark in the photographs, are seen in the optical microscope to have the characteristic color of the oxide (with minor variations), indicating that essentially all of the metal has been removed from these areas. Scanning electron micrographs[6] show a center hole, a few μm in diameter, in the oxide itself. With n-Si and negative field plate, multiple holes are frequently seen.

Figure 13 shows SQBDs produced in an oxide similar to the above but grown on p-type silicon. The breakdowns shown in Fig. 13(a) were produced at 100°K. The upper two, with irregular edges, were obtained by applying negative field-plate voltage (∿ 190 volts). Most striking, however, are the lower breakdown regions, which were produced by positive field-plate voltage (∿ 190 volts). These regions of field-plate removal are almost square, with their sides parallel to the [100] axes of the underlying silicon crystal. As with the n-type substrates, scanning electron micrographs[6] show center holes a few μm in diameter. Similar breakdowns, but produced at room temperature, are shown in Fig. 13(b). The breakdown regions encircled by the dashed lines were produced with the field plate positive. Here the edges are again smooth, but the square character is almost lost. In this photograph the remainder of the breakdowns, which have irregular edges, were produced by negative field-plate voltage.

In summary, the characteristics shown by the breakdown regions are as follows: (1) Positive field-plate voltage produces regions of field-plate removal that have smooth edges. The regions are circular in shape for n-type substrates but tend to be square, with the sides parallel to the [100] axes of the underlying crystal, for p-type substrates. (2) Negative field-plate voltage produces regions of field-plate removal that have irregular edges. (3) Each breakdown region has a center hole a few μm in diameter. Multiple holes were sometimes observed, particularly with n-type substrate and field plate negative. (4) Scratches on the field plate were found to nucleate breakdowns when the field plate was positive. Scratch nucleation was not observed with the field plate negative. (5) A further observation,

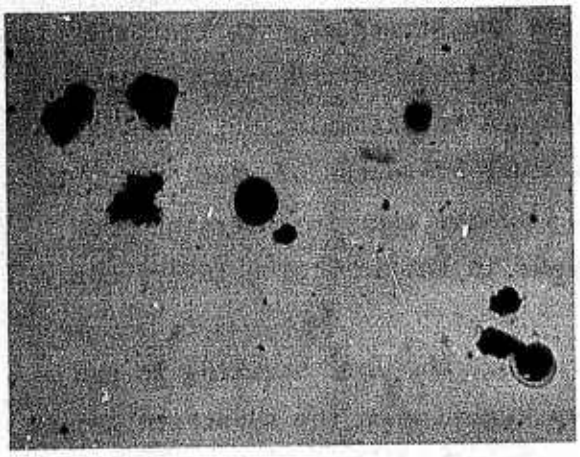

Fig. 12. Optical micrograph of SQBDs produced at 100°K. 2500-Å SiO_2, n-type substrate. Smooth-edged circles: Al(+). Irregular regions: Al(-). (400X.)

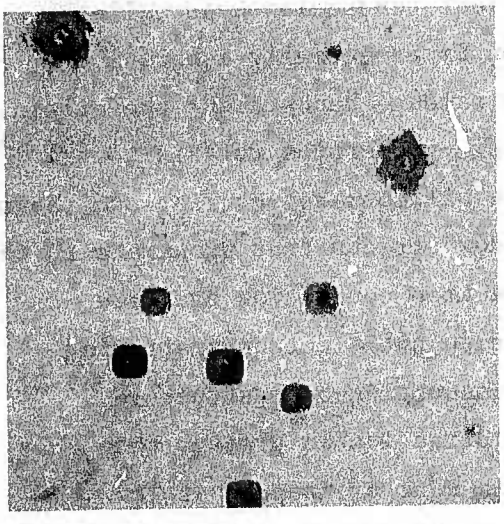

(a)

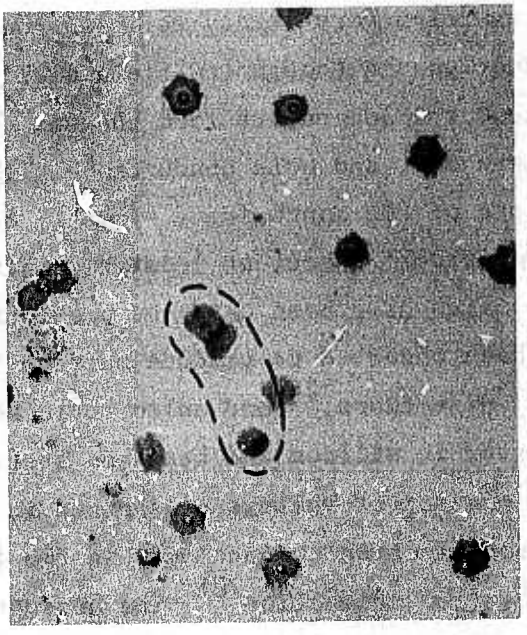

(b)

Fig. 13. Optical micrographs of SQBDs, 2500-Å SiO_2, p-type substrate. (a) Breakdowns produced at 100°K. Squares with smooth edges: Al(+). Irregular regions: Al(-). (b) Breakdowns produced at room temperature. Encircled with dashed line: Al(+). Irregular regions: Al(-).

obtained by monitoring the voltage across the structure, was that the time scale for removal of the field-plate material was of the order of 10 nsec for those situations where the substrate was in accumulation, and was considerably greater than this, of the order of tenths of μsec, when the substrate was in inversion. This indicates that in inversion the principal voltage drop in the structure is in the inversion layer, not across the fault in the oxide.

Of all the observations described above, the most striking is the anisotropy shown by the square breakdown region when the substrate is p-type and the field plate is positive. It will be noted that although the substrate is in inversion under this condition, a corresponding anisotropy is not seen with an n-type substrate and negative field-plate polarity. The anisotropy of the breakdown configuration observed with (100) p-silicon in inversion very likely derives from the anisotropy of hot-electron conduction. Although low-field electron conduction in silicon is isotropic because the components from the six equivalent conduction-band valleys average out, and hole conduction in silicon is essentially isotropic because of the approximate symmetry of the valence bands about the origin in reciprocal space, at least two anisotropic properties related to the [100] axes have been observed previously in silicon: hot-carrier excitation has been observed to produce surface breakdown tracks that propagate in the [100] directions,[28] and anisotropic hot-electron conduction has been observed in silicon and has been attributed to hot-electron scattering from one set of valleys to another in the conduction-band structure.[29-31] The hot-electron conductivity in the [110] direction is greater than that in the [100] direction.[31] The anisotropy is more pronounced at low temperatures than at high temperatures. An explanation for the observed anisotropic breakdown is as follows: When the insulating film suffers a local breakdown, the collapse of the voltage at the fault results in the appearance of a large radial electric field in the inversion layer in the immediate vicinity of the breakdown. The Joule heat produced by hot-electron conduction in the inversion layer vaporizes the field plate. The higher hot-electron conductivity in the [110] direction produces a greater evolution of heat along the [110] axes and removes more metallic

material along these directions.

In order to study the effect on the anisotropy of an increased electric field, we prepared samples with thicker oxides, thus increasing the electrostatic energy stored in the oxide at the breakdown field intensity. These samples consisted of 3000 Å and 4000 Å HCl-steam-grown oxides on p-type (100) silicon substrates. Very thin aluminum field plates, a few hundred Å in thickness, were used in order to produce minimal interference with the heating contour. Typical results obtained at room temperature with a 4000 Å oxide are shown in Fig. 14. The breakdown voltages here ranged up to 280 volts. It is seen that the increased electric field applied to the inversion region upon breakdown has accentuated the anisotropy and has resulted in four-pointed star configurations of field-plate removal with the points of the stars aligned in the [110] directions of the underlying silicon crystal. When defects and weak spots are present in the oxide, the breakdown voltage varies from one place to another across the sample, and this provides an opportunity to observe a variety of SQBDs as the applied voltage is gradually increased. The evolution in shape can be seen clearly in the photograph of Fig. 15, which was taken at room temperature on a 4000 Å oxide. Three SQBDs appear here, apparently nucleated on a scratch on the field plate. The respective breakdown voltages were 170 volts for the circle, 200 volts for the square, and 230 volts for the star. This picture demonstrates clearly the field dependence of the anisotropy.

3.3. A Slow High-Field Instability

During the course of our work we observed and investigated a slow instability which leads to breakdown in Al-SiO_2-(100) Si structures and whose progress is enhanced at lowered temperatures. A similar instability has been reported by Osburn and Weitzman.[32] We find that when we subject the structure to a voltage just below the value which will cause immediate breakdown, using either polarity, a small current initially flows which can be attributed to the tunneling of electrons from whichever electrode is negative (References 25, 32 and Sections 2.5 and 2.6 of this report). The current gradually increases over a period of time whose duration is critically dependent on the exact value of the applied voltage: it can be

minutes or an hour or more. This long-term instability eventually results in some SQBDs and finally terminates in a series of rapid breakdowns which destroy the sample if the voltage is not removed. Two further observations are of importance. First, positive charge is found to build up in the insulator as the instability progresses. Second, if the sample is cooled (toward liquid nitrogen temperature) the instability progresses at a faster rate. Typical results obtained while cooling the sample in vacuum are shown in Fig. 16. The sample here was a 2500 Å film of SiO_2 which had been HCl-steam-grown on (100) silicon of 1-2 Ω-cm resistivity, using an aluminum field plate of approximately 1000 Å thickness. With a voltage of +190 V applied to the field plate, the current increased slightly for about 20 min but stabilized. As the sample was cooled toward liquid nitrogen temperature the current showed a slight decrease. In contrast with this is the result obtained with a voltage of +195 V applied to the field plate, as shown by the top curve. The current showed an initial rise at room temperature but stabilized. As cooling was started the current showed an initial decrease, but at temperatures below about -75°C the current increased continuously and the sample underwent a few SQBDs as indicated by the spikes on the curve. Finally after about 150 minutes, with the sample at a temperature of approximately 90°K, a rapid series of SQBDs took place and the voltage was removed to preserve the remainder of the sample. Similar results were obtained (on fresh samples) with negative voltage applied to the field plate, the voltage required for instability being slightly less than for positive polarity (∿ 185 V). The same instability was observed with oxides grown on both p and n substrates.

The charge storage observed in the oxide is illustrated by the C-V curves of Fig. 17, which were taken at a frequency of 1 MHz. Curve 1 is the original C-V characteristic. The sample was then brought to the verge of instability by applying +190 volts to the field plate, and the bias was maintained for one hour. During this time a steady-state current, attributable to the tunneling of electrons from the substrate, was observed. At the end of this period the C-V curve labeled 2 was measured, showing a storage of positive charge in the oxide. Curves 3 and 4 show how the

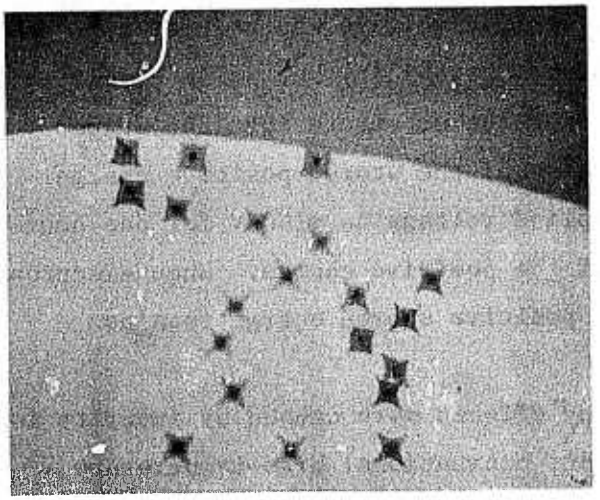

Fig. 14. Optical micrograph of anisotropic SQBDs produced at room temperature, 4000-Å SiO_2. p-type substrate, Al(+). The points of the stars line up with the [110] directions. (100X.)

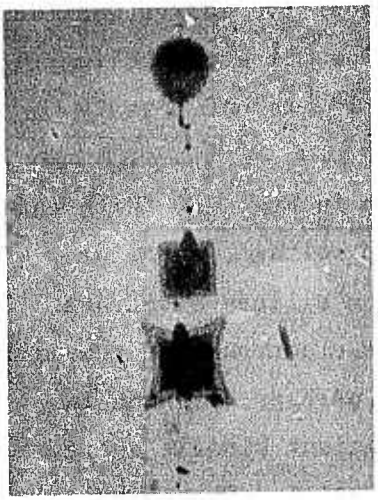

Fig. 15. Optical micrograph of SQBDs produced at room temperature, 4000-Å SiO_2, p-type substrate, Al(+). The breakdown voltages were 170 V for the circle, 200 V for the square, 230 V for the star. The sides of the square are parallel to the [100] directions. (400X.)

positive stored charge can be annealed out by an injection of electrons from the substrate. For Curve 3 the applied voltage was reduced to +150 V, which is well below the point of instability but still sufficient to cause the tunneling of electrons from the substrate into the oxide. After three hours an appreciable portion of the stored positive charge had been removed. An increase in applied voltage to +160 V for one hour produced a still further annealing of the positive charge. When electrons are not injected into the oxide, the positive stored charge remains indefinitely.

The possibility that the observed effects were caused by impurity ion contamination was investigated. First, conventional bias-temperature stress measurements were performed, and these indicated negligible ionic contamination. Second, after positive charge was stored by bringing the sample to the verge of instability, the sample was heated to a temperature of 300°C, meanwhile maintaining a voltage of +50 V on the field plate. This treatment should have held any positive ions at the Si-SiO_2 interface and the positive charge, if caused by ions, should have been maintained. However, the reverse effect was observed, and the positive charge was found to anneal out. Finally, the electron annealing of positive charge in silicon dioxide, in the manner illustrated in Fig. 17, is undoubtedly a characteristic of trapped holes, not of ions.

The observed results can be explained as shown in Fig. 18. With the field plate biased to a sufficiently large positive voltage, a Fowler-Nordheim tunneling of electrons takes place from the silicon substrate into the conduction band of the oxide. Most of the electrons are thermalized near the bottom of the conduction band, but a few, perhaps only one in about 10^3 according to our estimates, acquire sufficient kinetic energy to cause hole-electron pair production by impact ionization. The holes drift toward the Si-SiO_2 interface where some of them are trapped, and the resulting positive space charge enhances the electric field at the interface and increases the tunneling of electrons. Incoming electrons tend to recombine with the trapped holes, and instability arises only when the production and trapping of holes dominates over recombination. As the temperature is lowered, the fraction of electrons that can reach the required large kinetic energy is increased and the instability is enhanced.

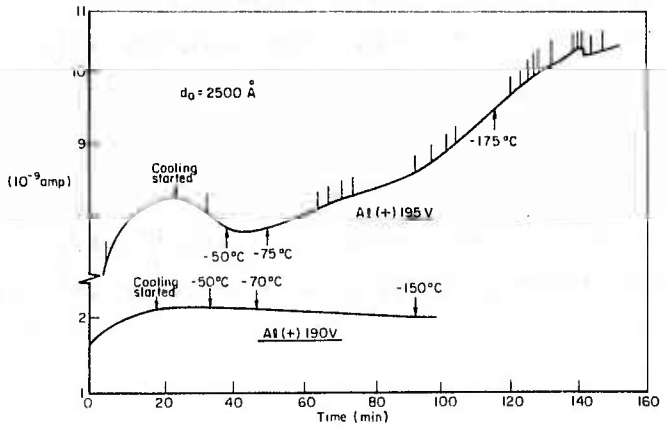

Fig. 16. Current vs. time, with cooling started after stabilization of current. The lower curve shows stability; applied voltage is 190 V. The upper curve shows instability which arises as temperature is reduced; applied voltage is 195 V.

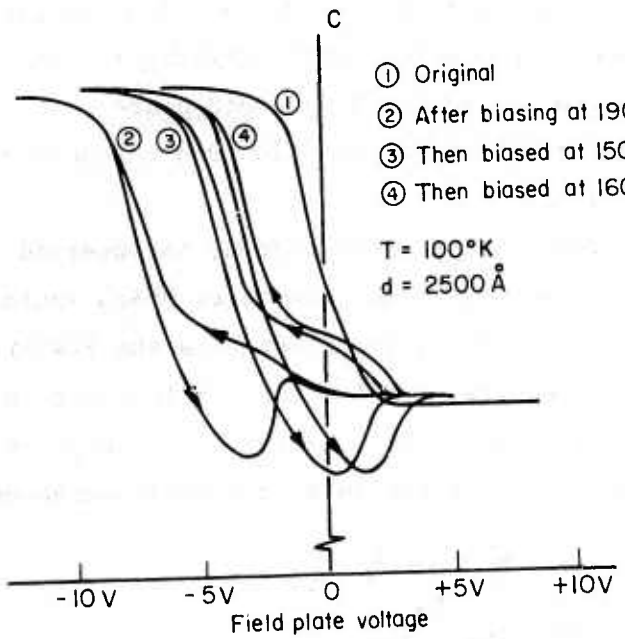

Fig. 17. High-frequency C-V curves showing positive charge buildup in the oxide associated with instability; and electron-current annealing of the positive charge at somewhat reduced voltages.

Inasmuch as we observe an exactly similar instability when the field plate is biased to a negative potential, we are led to suppose that processes similar to those shown in Fig. 18 take place but with the roles of the two electrodes interchanged. Positive charge trapped under the field plate can not be observed by C-V measurements because the charge is imaged in and shielded by the metal. Our C-V measurements indicate negligible storage of charge in the bulk of the oxide or at the $Si-SiO_2$ interface after instability has been induced by applying a negative voltage to the field plate.

3.4. Conclusions

Observations of SQBDs in $Al-SiO_2$-(100) Si structures show distinct differences in the breakdown regions produced with n-type and p-type substrates and with positive and negative field plate polarities. The boundaries of field-plate removal are smooth for positive field-plate polarity and irregular for negative field-plate polarity. Scratch nucleation takes place only when the field plate is positive. Most striking is the anisotropy obtained with p-type substrates and positive field-plate polarity. This is attributed to the anisotropy of hot-electron conduction in the inversion layer of the substrate.

A slow instability, eventually terminating in breakdown, is observed when the structure is biased to a voltage just below the value which would cause immediate breakdown. A model is presented which includes the Fowler-Nordheim tunneling of electrons from the negative electrode, hole-electron pair production by a few electrons which reach the required high energy in the oxide, and trapping of holes near the negative interface which enhances the electron tunneling.

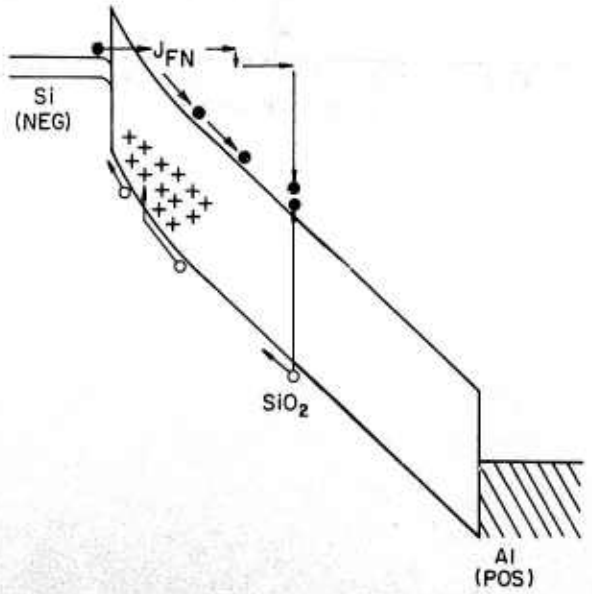

Fig. 18. Schematic energy-band diagram showing a possible series of mechanisms causing instability. J_{FN} is a Fowler-Nordheim tunneling of electrons from the negative electrode. A few electrons reach high energies and cause hole-electron pair production. Holes are trapped near the negative interface, enhancing J_{FN}.

4. GENERATION OF ELECTRON TRAPS IN SiO_2 BY ION IMPLANTATION AND BY ELECTRON IRRADIATION*

4.1. Introduction

Normal thermally grown silicon dioxide has only small concentrations of electron traps[21] and electron trapping is ordinarily negligible. Electron traps can be generated, however, during the use of the devices and circuits employing silicon dioxide as the insulator, and the space charge of electrons in these traps can substantially alter the device characteristics and the breakdown properties of the oxide. The discovery that electron trapping centers are generated in silicon dioxide under high-field conditions has already been discussed in Sec. 2.7 of this report. In the present section we present the results of experiments which show that electron traps are also generated in silicon dioxide by aluminum ion implantation and by electron irradiation.

4.2. Generation of Electron Traps by Aluminum Ion Implantation

(N. M. Johnson collaborating)

A. Summary

In this study we used photoelectric and MOS capacitance-voltage techniques to investigate electron trapping in aluminum-implanted SiO_2 and to compare the trapping with that observed in unimplanted control samples. The results showed that the aluminum implantation created large concentrations of electron traps in the oxide. A substantial fraction of the electron traps were associated with the displacement damage introduced by the ion implantation, as was indicated by (1) a considerable reduction in electron trapping when the implanted sample was thermally annealed, and (2) similar electron trapping found in preliminary studies of argon-implanted oxides. The implantation of other species of ions is expected to produce similar electron trapping centers.

B. Experimental Procedure

Our samples were fabricated from a 3-Ω cm n-type silicon wafer with (100) crystal orientation. The oxide layer was grown in dry oxygen at 1000°C to a thickness of 1400 Å. The oxide of one section of the wafer was implanted with aluminum ions at 20 keV to a fluence of 10^{14} cm^{-2}. The other section was not implanted and served as a control sample. Semitransparent

* This work was also supported in part by the Defense Nuclear Agency under the sponsorship of the Naval Research Laboratory/Office of Naval Research.

gold field plates were vacuum deposited on the exposed oxide surface. The samples received no heat treatment prior to the beginning of our experiments.

The experimental procedure that we used to study the electron traps in the oxide was as follows. The metallic field plate of the sample was biased positively with respect to the silicon substrate, and the structure was illuminated from the front with photons having an energy smaller than the oxide band gap but greater than the electronic barrier between the silicon substrate and the oxide. For this purpose we used photons with an energy of 4.8 eV. A substantial fraction of the incident photons penetrated the semitransparent field plate and passed through the oxide to the $Si-SiO_2$ interface where they stimulated an internal photoemission of electrons from the silicon into the conduction band of the oxide. These electrons were then drifted by the electric field toward the positively biased field plate and were subject to capture by electron traps in the oxide. The storage of negative charge resulting from electron capture produced a shift in flatband voltage which could be determined from the high-frequency MOS capacitance-voltage (C-V) characteristic. Subsequent discharge of the traps could be accomplished by photodepopulation or by thermal annealing with the contacts short circuited.

C. Results

The unannealed aluminum-implanted samples initially displayed flatband voltages of approximately -15 V, indicating an initial storage of positive charge. In contrast, the control samples showed only small initial flatband voltages, typically - 1 V. The positive space charge in the implanted samples was neutralized almost completely, and the flatband voltage was brought essentially to zero, by irradiating the sample with 4.8 eV photons with the contacts short circuited. Alternatively, the initial positive charge could be removed by thermal annealing at 450°C for 30 min with the contacts short circuited.

After the initial positive charge had been neutralized, the electron trapping properties of the oxide were investigated by biasing the field plate positively and illuminating the sample to produce an internal photoemission of electrons from the substrate. The sample current was monitored and, at intervals, the high-frequency (1 MHz) C-V characteristic of the sample was measured to determine the charge storage. Typical results of such an experiment are shown in Figs. 19 and 20. Here the field-plate

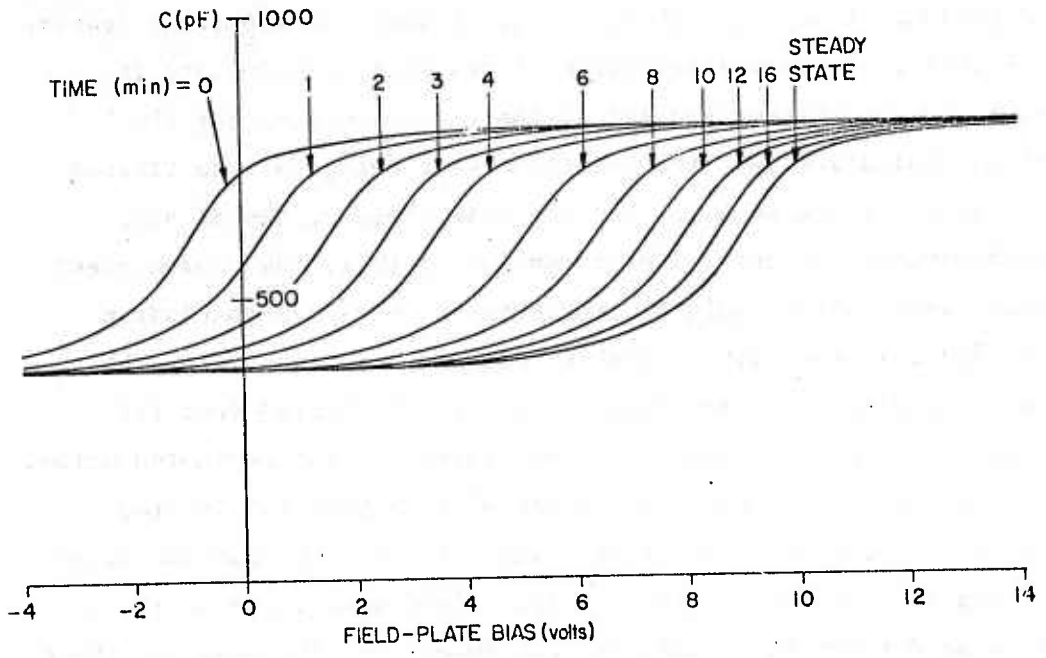

Fig. 19. Voltage shifts of the C-V curve with time during electron photoinjection. The sample voltage was maintained at V_S = 10 V with the field plate positive during photoinjection.

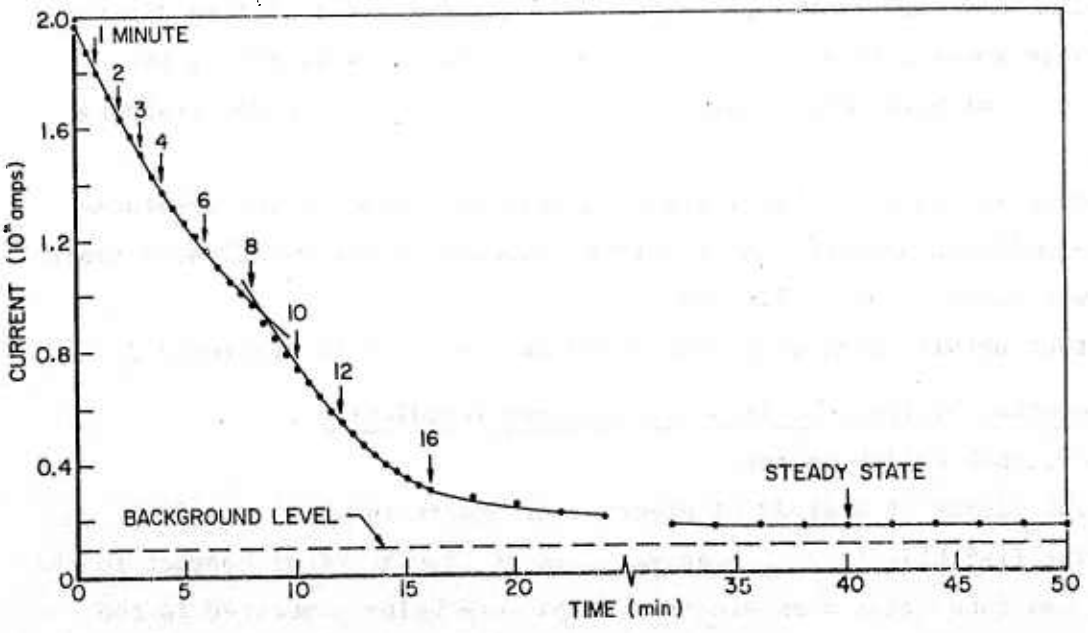

Fig. 20. Photocurrent transient during electron photoinjection with sample voltage maintained at 10 V. Arrows indicate when light was interrupted to record the C-V curves shown in Fig. 1.

voltage was held at + 10 V during photoinjection. As is shown in Fig. 19, the C-V curves shifted to the right as the photoinjection proceeded, indicating a buildup of negative charge in the oxide. An important feature in Fig. 19 is that the steady-state value of the flat-band voltage is virtually equal to the voltage applied to the field plate during the photoinjection, indicating that the negative space charge of the trapped electrons was great enough to bring the electric field at the Si-SiO_2 interface approximately to zero. Corresponding to this, the photocurrent fell to a small value which could be attributed to stray photoemission from other surfaces in the sample chamber (Fig. 20). An analysis, the details of which are given in References 3 and 15, indicated that (1) essentially all injected electrons had been trapped in the implanted oxide, (2) that the centroid of the negative charge distribution was located approximately 670 Å from the field plate, and (3) that the observed decay in current could be explained by the electric-field dependence of the photoinjection as determined by Berglund and Powell.[33] The negative space charge in the implanted samples could be annealed either optically by photons of energy exceeding 4 eV or thermally at 350°C. A 600°C anneal for 30 min substantially reduced the concentration of electron traps, indicating that many, perhaps most, of the traps were associated with displacement damage introduced by the ion implantation.

Preliminary experiments on unannealed neon-implanted silicon dioxide showed large amounts of electron trapping, further substantiating the importance of displacement damage in the production of electron trapping centers.

In contrast with the heavy electron trapping found in the aluminum- and neon-implanted samples, the electron trapping in the unimplanted control samples was found to be negligible.

Further details regarding this study can be found in Reference 3.

4.3. Generation of Electron Traps by Electron Irradiation

(C. T. Shih collaborating)

In the course of a study of electron transport in which a non-penetrating (1-5 kV) electron beam was used as an electrical contact to the SiO_2, it was found that deep electron traps were being generated in the

insulator by the electron irradiation. Further study showed that the traps were not confined to the volume of the insulator in which the electrons stopped, but existed through the entire thickness of the SiO_2.

The existence of the electron trapping centers was first deduced from the structure of the steady-state I-V curves and was then confirmed by experiments designed to alternately charge and discharge the traps. The results of a typical experiment are shown in Fig. 21 for a 4700 Å oxide. Curve 1 is the initial C-V curve taken at 1 MHz. Curve 2 shows the effect of irradiation with an electron beam that deposited most of its energy within the first 2000 Å of the oxide. The stretch-out of the curve indicates the presence of interface states. Curve 3 shows the result of an anneal which removed most of the interface states. The effect of negative charge storage, presumably in electron traps, is now shown clearly. Curve 4 shows the result obtained by photoinjecting electrons from the substrate into the SiO_2. Some of the electrons were trapped, increasing the negative charge storage. Curve 5, showing additional negative charge storage, was obtained by an additional photoinjection of electrons, this time from the metal field plate. As is shown by Curve 6, most of the negative trapped charge could be annealed out at 350°C. The traps themselves remained, however, and could be recharged by photoinjecting electrons again, thus restoring the positive flatband shift. The structure of steady-state I-V curves and the voltage dependence of electron photoinjection currents indicated that the electron trapping was in the bulk of the oxide and that a substantial portion of it was located well ahead of the range of the irradiating electrons. The saturated concentration of the electron traps was found to be in excess of 10^{17} cm^{-3}.

The detailed nature of the electron traps is not known, but their presence has important implications in regard to the results obtained from electron-beam studies of the SiO_2.

Further details regarding this study can be found in Reference 16.

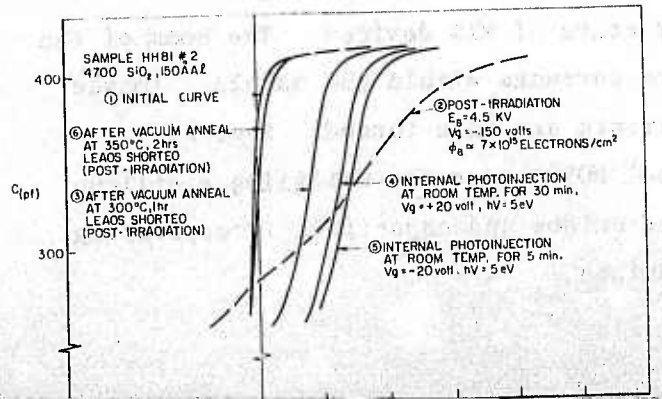

Fig. 21. Evidence of electron trapping in SiO_2 irradiated by a nonpenetrating electron beam.

5. STUDIES OF LATERAL NONUNIFORMITIES IN MIS STRUCTURES

5.1. Introduction

The importance of interface states and of charge storage in the metal-insulator-semiconductor (MIS) structure was recognized early. Charge storage produces a shift in the capacitance-voltage (C-V) characteristics along the voltage axis and a change in turn-on voltage. Interface states produce a stretch-out of the C-V curves and also alter the turn-on voltage. The effects of these are generally analyzed by modeling the charge storage and the interface states in a one-dimensional, laterally uniform manner. More recently, however, it has been recognized that lateral nonuniformities, such as nonuniformities in charge storage, insulator thickness, or substrate doping, can cause a stretch-out in the C-V curves and alter the turn-on voltage in much the same manner as interface states. In fact, it now appears likely that some of the difficulties formerly blamed on interface states might have been caused instead by lateral nonuniformities. Thus it becomes important to develop diagnostic techniques for the identification of nonuniformities and methods of characterizing them when they are found. We have conducted two distinct studies of this problem, utilizing totally different techniques. In one, we have developed methods for using the scanning electron microscope to image the insulator and the insulator-semiconductor interface in order to study and identify nonuniformities. In the other, we have developed techniques by which electrical measurements made at the terminals of an MIS capacitor can be used to determine the presence of lateral nonuniformities in the structure, and we have devised a simple but effective method for characterization of the nonuniformities. The two studies are described below.

5.2. Scanning-Electron-Microscope Studies of Nonuniformities

(D. Guterman and P. Roitman collaborating)

We have developed a technique for utilizing the scanning electron microscope to image the internal structure of MIS devices. The beam of the electron microscope is used to induce currents within the sample. Images sensitive to variations in these currents are thus formed. Most of the samples studied have been conventional MOS structures utilizing a silicon dioxide insulator; however, implanted oxides and capacitors incorporating Al_2O_3 dielectric films were also examined.

We have developed a theoretical foundation for determining the range and ultimate spatial resolution for the incident beam and have analyzed three sources of induced current: (1) electron-beam-induced conductivity (EBIC) within the insulator, (2) internal emission over the insulator-interface barrier, and (3) displacement currents generated within the depletion region of the substrate.

The experimental techniques that we have employed include induced-current imaging studies and single-line scans as a function of incident energy, current, scan speed, and applied bias. Information derived from backscattered primary and secondary electron imaging supplements that of the induced currents. Supporting techniques such as capacitance-voltage, current-voltage, bias-thermal stress (BTS), and self-quenching breakdowns were employed to clarify the nature of observed features.

Two types of structure were studied in detail. Stacking faults in the substrate which terminate at the Si-SiO_2 interface were found in a number of MOS capacitors. Qualitative agreement between observed and theoretical current dependence was demonstrated. Carrier-lifetime variation within faulted regions is proposed as a possible source of their contrast. The second type of structure, ion aggregations (very likely sodium), were observed within SiO_2, adjacent to an interface, after extended bias-thermal stressing of MOS samples. The location, density and size of these structures was shown to be dependent on sample preparation and BTS history. Their contrast in beam induced imaging is proposed to arise from either enhanced conductivity within the SiO_2 or enhanced internal emission over the interface barriers, depending on the imaging parameters. An example of the EBIC imaging of sodium clusters at an Si-SiO_2 interface is shown in Fig. 22. Formations observed in other samples include defects incorporated during processing and damage introduced by ion implantation.

Under certain conditions a beam-structure interaction is observed, indicating that radiation damage produced by the electron beam can have a significant effect on the images. Although such radiation damage is seen to influence both the structures and their images, it is concluded that the induced imaging technique that we have developed is of significant value in the analysis of internal structures within MIS devices.

Further details regarding this study can be found in References 13, 14, and 19.

5.3. Study of Lateral Nonuniformities by Electrical Measurement Methods

(C. C. Chang collaborating)

Although this study was funded from other sources,* we include it here because of its importance to the other segments of our program.

The performance of solid-state devices and circuits based on the metal-insulator-semiconductor (MIS) structure is adversely affected by the presence of either interface states or lateral nonuniformities. The study of lateral nonuniformities is handicapped by the fact that their effect on the C-V characteristics of the structure resembles that of interface states. In this work we have studied methods for distinguishing between lateral nonuniformities and interface states and for characterizing lateral nonuniformities when these are determined to be present.

We have devised a simple, approximate method for determination of the distribution of flat-band voltages in a nonuniform MIS capacitor, using only the measured quasi-static and high-frequency C-V curves of the structure. Computer simulation indicates that the approximate formula generally yields acceptable results. We also propose a more exact method based on use of the Fast Fourier Transform technique.

We have developed two methods for distinguishing between interface states and lateral nonuniformities which are based respectively on the frequency dependence of interface-state capacitance and on the temperature dependence of both minority-carrier generation and emission from interface states. Experimental results illustrate the feasibility of these methods.

Analysis shows that when a C-V stretch-out is caused by lateral nonuniformities, the resulting quasi-static and high-frequency C-V curves cannot both be fitted by any distribution of interface states, and, conversely, if the stretch-out is caused by interface states, the resulting quasi-static and high-frequency C-V curves cannot both be fitted by an lateral distribution of flat-band voltages. A convenient procedure for utilizing this principle has been devised and proved experimentally.

A study of interface states generated under high-field conditions in metal-silicon dioxide-silicon capacitors indicates that these states have their charge-neutral level approximately at silicon mid-gap. This study was made possible by the observation that application of the high

---

* This study was supported in part by Bell Telephone Laboratories, Inc.

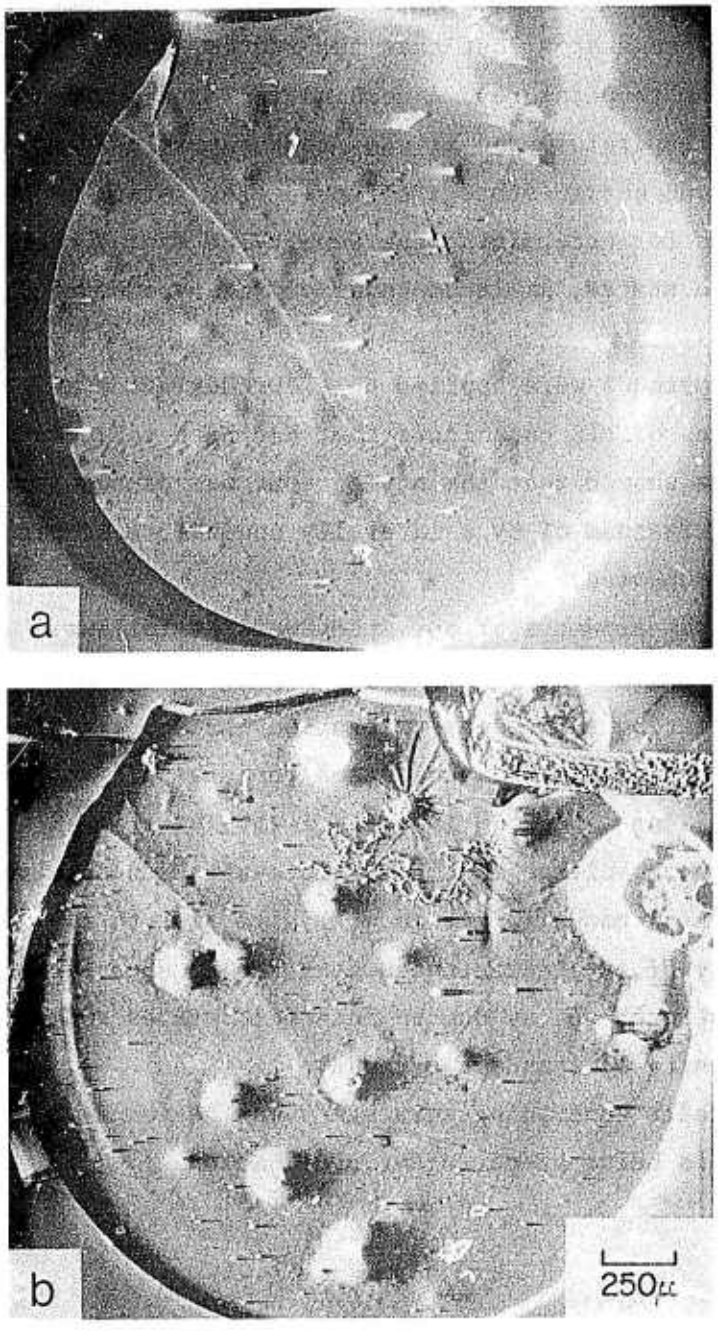

Fig. 22. EBIC images of an MOS structure taken (a) prior to bias thermal stressing, and (b) after bias thermal stressing for 13.5 hrs. at 175°C, and V_g = + 50 V. Cone-like structures are observed in the induced-current image after stressing.

field at liquid-nitrogen temperature does not result immediately in the generation of interface states, but that the states develop as the sample is warmed toward room temperature. A combination of experiments performed at liquid-nitrogen temperature and at room temperature permitted separation of interface-state and charge-storage effects. The foregoing result provides a reference for determining the density of stored charge in the oxide when interface states, at least those of the type we studied, are present.

The foregoing methods were applied to a further study of the stretch-out of the C-V curves of MIS capacitors that had been subjected to high fields. The results showed that the stretch-out was caused by the generation of interface states instead of by a laterally nonuniform storage of charge, as might have been supposed.

Two additional by-products of our study were as follows: (1) We found it to be generally true that the principal source of minority carriers in the depletion regime was generation through interface states, while in the inversion regime the generation through bulk states was dominant. This explains a peak in the relatively low-frequency C-V curves near the turn-on voltage that has frequently been observed. (2) The presence of lateral nonuniformities will give rise to two apparent peaks in the density of interface states near the band edges if one misinterprets the stretch-out as due to interface states and obtains the interface-state density by standard methods.

Additional details concerning this study can be found in Reference 34. This material is being prepared for publication.

6. THEORETICAL MODELING

6.1. Modeling of Electrical Breakdown in SiO_2 Films

(Dr. Brian K. Ridley collaborating)

The breakdown field associated with impact ionization and avalanche was estimated, using simple energy-momentum balance equations, for low-gap semiconductors and for high-gap insulators. Reasonable agreement was obtained in the former case, but estimated fields in the latter case turned out to be nearly an order of magnitude higher than those observed. This suggests that mechanisms other than avalanche are responsible for breakdown in insulators. A mechanism for SiO_2 films, based on Fowler-Nordheim injection from a cathodic protuberance, filamentary Joule heating, and activation of mobile positive ions, which enhance the injecting field, was explored. The protuberance was taken to be spheroidal, with a dimension related to the thickness of the film and of order 100 Å. A mechanism for lateral spreading of the initial discharge and subsequent quenching by the substrate resistance gives the extent of the damaged area to be of the observed order in self-healing breakdowns. The breakdown field and its dependence on film thickness are in reasonable agreement with experiment.

A detailed discussion of this study can be found in Reference 12.

6.2. Hot-Electron Distributions in Insulating Films

(Professor M. A. Lampert collaborating)

The hot-electron energy distribution produced in a high electric field, F, across a thin insulating film was studied by Monte Carlo calculations on a digital computer. The dominant electron collisions were assumed to be those with the lattice, producing single optical-phonon emissions of energy ε_{ph}. The mean free path λ was initially taken as a constant independent of energy, and both isotropic and anisotropic scattering were studied. A scaling law for the average electron energy $E_{ave,ss}$ in the steady-state distribution, previously found analytically for isotropic scattering, namely $E_{ave,ss} = k(F\lambda)^2/\varepsilon_{ph}$, was found to hold also for anisotropic scattering, k being a numerical constant determined by the detailed nature of the scattering law. Forward scattering produces larger values of k, backward scattering smaller values. No matter how strongly

peaked the forward scattering, short of exact ($\theta=0$) forward scattering, there is a finite, steady-state distribution. An analogous scaling law was found for the development distance D required to achieve the steady-state distribution, namely $D = k'(F\lambda^2)/\varepsilon_{ph}$.

Since the study of anisotropic scattering is costly, an extensive computer study was made of a highly simplified simulation, namely a one-dimensional random walk (fixed path length between collisons) in a force field. The salient features of the three-dimensional energy distribution are reproduced by the one-dimensional simulation, and the computer running time is reduced by a full order-of-magnitude.

A paper giving the results of the foregoing study has been accepted for publication.[35] In preparation is a second paper giving the results of a study showing that when the mean free path of the electrons increases with increasing energy, some of the electrons escape from the well behaved part of the distribution and gain large energies. This is of importance in impact ionization (Section 3.3).

REFERENCES

A. Publications, Reports, and Doctoral Dissertations Resulting From Work Done Under This Contract

1. M. A. Lampert, W. C. Johnson, and W. R. Bottoms, "Study of Electronic Transport and Breakdown in Thin Insulating Films," Semi-Annual Technical Report No. 1 (AFCRL-TR-73-0263), January 1973.

2. M. A. Lampert, W. C. Johnson, and W. R. Bottoms, "Study of Electronic Transport and Breakdown in Thin Insulating Films," Semi-Annual Technical Report No. 2 (AFCRL-TR-74-0076), July 1973.

3. N. M. Johnson, W. C. Johnson, and M. A. Lampert, "Electron Trapping in Ion-Implanted Silicon Dioxide Films on Silicon," Special Report No. 1 (AFCRL-TR-74-0133), January 1974. (This Special Report was based on N. M. Johnson's doctoral dissertation. The work described in this report was supported partially under this program and partially by other sources.)

4. W. C. Johnson, M. A. Lampert, and W. R. Bottoms, "Study of Electronic Transport and Breakdown in Thin Insulating Films," Semi-Annual Technical Report No. 3 (AFCRL-TR-74-0229), January 1974.

5. Z. A. Weinberg, W. C. Johnson, and M. A. Lampert, "Determination of the Sign of Carrier Transported Across SiO_2 Films on Silicon."
   (a) Appl. Phys. Lett. 25, 42 (1974).
   (b) Special Report No. 2 (AFCRL-TR-74-0206), April 1974.

6. D. Y. Yang, W. C. Johnson, and M. A. Lampert, "Scanning Electron Micrographs of Self-Quenched Breakdown Regions in Al-SiO_2-(100) Si Structures."
   (a) Appl. Phys. Lett. 25, 140 (1974).
   (b) Special Report No. 3 (AFCRL-TR-74-0278), June 1974.

7. W. C. Johnson and W. R. Bottoms, "Study of Electronic Transport and Breakdown in Thin Insulating Films," Semi-Annual Technical Report No. 4 (AFCRL-TR-74-0574), July 1974.

8. Z. A. Weinberg, "High-Field Transport in SiO_2 Films on Silicon Induced by Corona Charging," Ph.D. Dissertation, Princeton University, Sept. 1974.

9. D. Y. Yang, W. C. Johnson, and M. A. Lampert, "A Study of the Dielectric Breakdown of SiO_2 Films on Si by the Self-Quenching Technique," Special Report No. 4 (AFCRL-TR-74-0516), October 1974. (This Special Report was based on D. Y. Yang's doctoral dissertation.)

10. Z. A. Weinberg, D. L. Matthies, W. C. Johnson, and M. A. Lampert, "Measurement of the Steady-State Potential Difference Across a Thin Insulating Film in a Corona Discharge."
    (a) Special Report No. 5 (AFCRL-TR-74-0315), October 1974.
    (b) Rev. Sci. Instrum. 46, 201 (1975).

11. W. C. Johnson and W. R. Bottoms, "Study of Electronic Transport and Breakdown in Thin Insulating Films," Semi-Annual Technical Report No. 5 (AFCRL-TR-75-0157), January 1975.

12. Brian K. Ridley, "Mechanism of Electrical Breakdown in SiO_2 Films."
(a) J. Appl. Phys. 46, 998 (1975).
(b) Special Report No. 6 (AFCRL-TR-75-0182), March 1975.

13. W. R. Bottoms, D. Guterman, and P. Roitman, "Contrast Mechanisms in Electron Beam Images of Interface Structures."
(a) Special Report No. 7 (AFCRL-TR-75-0267), May 1975.
(b) J. Vac. Sci. Technol. 12, 134 (1975).

14. W. R. Bottoms and D. Guterman, "Electron Beam Probe Studies of Semiconductor-Insulator Interfaces."
(a) Special Report No. 8 (AFCRL-TR-75-0326), May 1975.
(b) J. Vac. Sci. Technol. 11, 965 (1974).

15. N. M. Johnson, W. C. Johnson, and M. A. Lampert, "Electron Trapping in Aluminum-Implanted Silicon Dioxide Films on Silicon," J. Appl. Phys. 46, 1216 (1975).

16. C. T. Shih, "A Study of the Effects of Low-Energy Electron Irradiation on MOS Capacitors," Ph.D. Dissertation, Princeton University, June 1975. (This work was supported partially under this program and partially by other sources.)

17. D. Y. Yang, W. C. Johnson, and M. A. Lampert, "A Study of the Dielectric Breakdown of Thermally Grown SiO_2 by the Self-Quenching Technique," 13th Annual Proceedings on Reliability Physics (IEEE), p. 10 (1975).

18. Z. A. Weinberg, W. C. Johnson, and M. A. Lampert, "High-Field Transport in SiO_2 on Silicon Induced by Corona Charging of the Unmetallized Surface," J. Appl. Phys. 47, 248 (1976).

19. Daniel C. Guterman, "Electron-Beam Induced Imaging and Analysis of Internal Structure in the Metal-Insulator-Semiconductor Structure," Ph.D. Dissertation, Princeton University, November 1975.

B. Other References

20. R. Williams and M. H. Woods, J. Appl. Phys. 44, 1026 (1973).

21. R. Williams, Phys. Rev. 140, A569 (1965).

22. R. C. Hughes, Phys. Rev. Lett. 30, 1333 (1973).

23. R. H. Good, Jr. and E. W. Müller, in Handbuch der Physik (Springer-Verlag, Berlin, 1956), Vol. XXI, p. 176.

24. S. Flügge, in Handbuch der Physik (Springer-Verlag, Berlin, 1956), Vol. XVII, p. 155.

25. M. Lenzlinger and E. H. Snow, J. Appl. Phys. 40, 278 (1969).

26. M. H. Woods and R. Williams, J. Appl. Phys. 47, 1082 (1976).

27. (a) N. Klein, "The Maximum Dielectric Strength of Thin Silicon Oxide Films," IEEE Trans. Electron Devices, ED-13, 281 (1966).

(b) N. Klein, "The Mechanism of Self-Healing Electrical Breakdown in MOS Structures," IEEE Trans. Electron Devices, ED-13, 788 (1966).

(c) N. Klein and N. Levanon, "A-C Electrical Breakdown in Thin Silicon Oxide Films," J. Appl. Phys. 38, 3721 (1967).

28. G. G. Harman, "Topological Features of Hot Carrier Induced Anisotropic Breakdown on Silicon Diode Surfaces," J. Res. Nat. Bur. Stand. (U.S.), 73A, 321 (1969). We wish to thank W. M. Bullis and A. G. Lieberman for calling our attention to this work.

29. B. R. Nag, "Hot-Carrier D-C Conduction in Elemental Semiconductors," Solid-State Electr. 10, 385 (1967).

30. E. M. Conwell, High Field Transport in Semiconductors (Academic Press, New York, 1967).

31. M. Asche, B. L. Boitchenko and O. G. Sarbej, "Abhangigkeit der Anisotropie der electrischen Leitfahigkeit des Siliziums vom elektrischen Feld," Phys. Stat. Sol. 9, 323 (1965).

32. C. M. Osburn and E. J. Weitzman, "Electrical Conduction and Dielectric Breakdown in Silicon Dioxide Films on Silicon," J. Electrochem. Soc. 119, 603 (1972).

33. C. N. Berglund and R. J. Powell, J. Appl. Phys. 42, 573 (1971).

34. C. C. Chang, "Study of Lateral Nonuniformities and Interface States in MIS Structures," Ph.D. Dissertation, Princeton University, February 1976.

35. S. Baidyaroy, M. A. Lampert, B. Zee, and R. U. Martinelli, "Monte-Carlo Studies of Hot-Electron Energy Distributions in Thin Insulating Films - I: Constant Mean Free Path and a One-Dimensional Simulation," accepted for publication in J. Appl. Phys.

MISSION
of
Rome Air Development Center

RADC is the principal AFSC organization charged with planning and executing the USAF exploratory and advanced development programs for information sciences, intelligence, command, control and communications technology, products and services oriented to the needs of the USAF. Primary RADC mission areas are communications, electromagnetic guidance and control, surveillance of ground and aerospace objects, intelligence data collection and handling, information system technology, and electronic reliability, maintainability and compatibility. RADC has mission responsibility as assigned by AFSC for demonstration and acquisition of selected subsystems and systems in the intelligence, mapping, charting, command, control and communications areas.